FIRST RESULTS ON W AND Z^0 PHYSICS FROM THE 1988 UA2 DATA

The UA2 collaboration

Bern - Cambridge - CERN - Heidelberg - Milano

Orsay (LAL) - Pavia - Perugia - Pisa - Saclay (CEN)

Presented by :

K. HULTQVIST*)

CERN, Geneva, Switzerland

ABSTRACT

The UA2 detector has been substantially upgraded to match the higher luminosity provided by the upgraded CERN $p\bar{p}$ collider. A total integrated luminosity of 2.7 pb^{-1} was collected during the 1988 run. A brief description of the detector is given, followed by a discussion of the preliminary analyses of the W and Z^0 trigger streams.

---

* Now at the University of Stockholm

1. Introduction

The UA2 detector has been extensively modified[1] in order to achieve an improved performance matching that of the upgraded $p\bar{p}$ collider at CERN.[2] Emphasis was given to an improved measurement of missing transverse energy and to the improvement of the electron identification. A new data acquisition and multilevel trigger system were implemented in order to handle the increase in luminosity and data volume. In Section 2 a brief overview of the detector is given. A more detailed description of the electron identification in the new detector is presented in Section 3. In Sections 4 and 5 the W and Z^0 selections are described. The results are based on an integrated luminosity of 2.5 pb^{-1} out of the data accumulated during September-December 1988. Section 6 discusses the problem of measuring the W and Z^0 masses and a few conclusions are drawn in Section 7.

2. The UA2 detector

A cross-section of a quadrant of the UA2 detector is shown in Fig. 1. The central calorimeter covers the pseudorapidity interval $|\eta| < 1.0$ over the full azimuth. The forward regions are covered by end-cap calorimeters down to an angle of 6° with respect to the beam axis. Similarly to the central calorimeter, the end-caps consist of electromagnetic and hadronic compartments and are divided laterally into cells. In the end-caps the two cells closest to the beam axis ($2.5 < |\eta| < 3.0$ and $2.2 < |\eta| < 2.5$) cover 30° in azimuth while the other end-cap cells have constant segmentation $\Delta\phi = 15°$, $\Delta\eta = 0.2$. Each cell in the central calorimeter covers $\Delta\phi = 15°$, $\Delta\theta = 10°$. The electromagnetic compartment is a multilayer sandwich of lead and scintillator with a thickness of 17 radiation lengths (r.l.) in the central calorimeter and varying between 17.1 and 24.4 r.l., depending on the polar angle, in the end-caps. The hadronic compartment is a multilayer sandwich of iron and scintillator corresponding to about 4.5, 7 (central, end-caps) absorption lengths including the electromagnetic part. Each compartment is read out via two wavelength shifting plates placed on opposite sides of each cell.

All cells in the end-caps and the central calorimeter were calibrated (in 1986) with beams of electrons and pions. The calibration is monitored using ^{60}Co sources, energy distribution in minimum bias events and recalibration of individual modules. The aim is to achieve an accuracy of $\pm 1\%$ for the electromagnetic energy scale.

The central detector, situated inside the calorimeter, consists of several sub-detectors. The detectors most relevant for the present analysis, and hence described here in some detail, are the Scintillating Fibre Detector (SFD) and the End-Cap Proportional Tubes (ECPT).

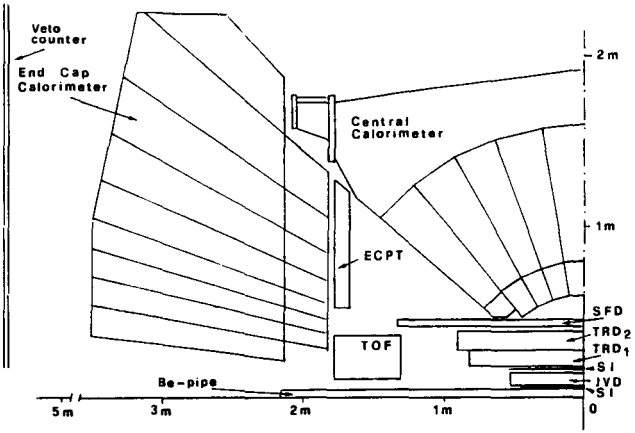

Figure 1. A cross-section of one quadrant of the upgraded UA2 detector (see text).

Figure 2. The distance between the extrapolated track and the preshower cluster in the SFD in (a) the $R\phi$-coordinate and (b) the z-coordinate (along the beam).

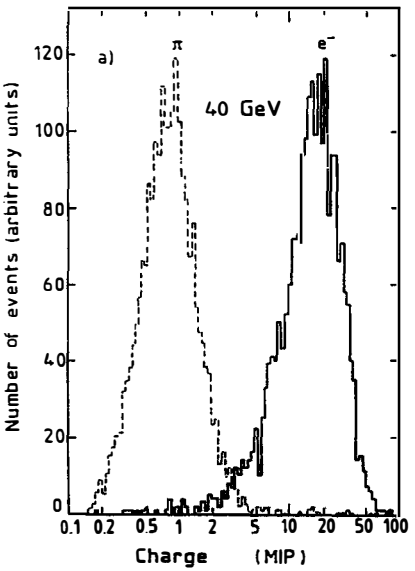

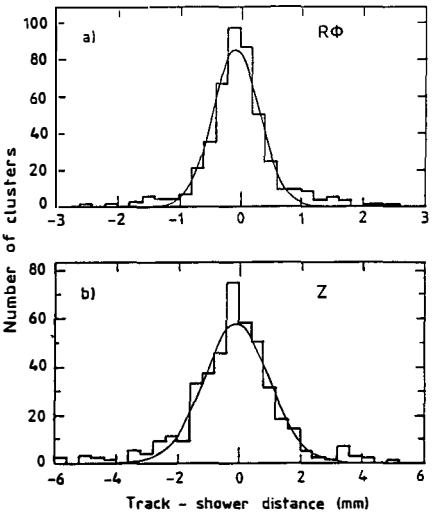

Figure 3. The charge distribution for the SFD preshower clusters for test beam data for 40 GeV electrons (solid line) and pions (dashed line), respectively. Note the logarithmic abscissa.

The **SFD**[3] is a tracking and preshower detector in front of the central calorimeter. The tracking part consists of 18 cylindrical layers of scintillating fibres (with a diameter of 1 mm) grouped in six stereo triplets. These tracking layers are surrounded by 1.5 r.l. of lead and two additional triplets which serve as a preshower detector. This detector gives a precise determination of the starting point of electromagnetic showers, discriminating against overlaps of charged pions and photons which could otherwise simulate electrons. In each stereo triplet one layer of fibres is parallel to the beam while the other two are inclined at angles $\pm\alpha$ where α is 15.75° for the tracking triplets and 21° for the preshower triplets. The tracking part covers the pseudorapidity region $-1.7 < \eta < 1.7$ while the lead converter covers only the region of the central calorimeter ($|\eta| < 1.0$).

The performance of the SFD is illustrated in Figures 2 and 3. Figures 2 a,b show the track-preshower matching along $r\phi$ and z for electrons from W $\rightarrow$ $e\nu$ decays. From the fitted widths, $\sigma(r\phi) = 0.4$ mm; $\sigma(z) = 1.1$ mm, one can define a normalised track-preshower distance, D, for each event :

$$D^2 = \left(\frac{\Delta(r\phi)}{\sigma(r\phi)}\right)^2 + \left(\frac{\Delta(z)}{\sigma(z)}\right)^2$$

where Δ is the distance between the track and the preshower cluster. The charge distributions for 40 GeV pions and electrons, as measured in a test beam, are shown in Fig. 3. In front of the end-cap calorimeters (Fig. 1) are the End-Cap Proportional Tubes (ECPT). In analogy to the SFD they are equipped with a 2 r.l. converter made of lead and iron. Each of the two ECPT detectors is divided into eight 45° azimuthal sectors and covers the polar angular range $22.5° < \theta < 37.5°$ (1.1 to 1.6 in pseudorapidity). Tracking is performed with 6 planes forming two stereo triplets at stereo angles 0, $\pm 67.5°$. The converter is followed by a single preshower triplet.

The resolution of the ECPT track-preshower matching is the same ($\sigma = 5$ mm) in the x and y directions (transverse to beam) and thus $D^2 = (\Delta(x)^2 + \Delta(y)^2)/25$ mm^2 in this case.

In addition to the tracking detectors already mentioned (the SFD and the ECPT) a cylindrical drift chamber, the Jet Vertex Detector (JVD), provides a track segment close to the interaction point. Two silicon detectors, one immediately outside the beam-pipe with 3072 pads ($\Delta\phi = 30°$, $\Delta z = 2$ mm) and one outside the JVD with 3024 pads ($\Delta\phi = 15°$, $\Delta z = 8.7$mm) provide two space points along the track and are also used as a fast vertex finder. These detectors measure the ionisation of charged particles and can be used to reject converted photons.

Outside the second silicon layer a Transition Radiation Detector (TRD) occupies most of the available space inside the calorimeter. Its purpose is to add discrimination power against hadrons simulating electrons for complicated event topologies.

In the forward direction close to the beam pipe are two Time-Of-Flight hodoscopes (TOF). They define a minimum bias interaction trigger and provide an independent vertex measurement.

3. Electron identification

Calorimeter clusters are obtained by joining all cells which share a common side and contain energy above 0.4 GeV. An *electromagnetic cluster* is defined by requiring that the cluster have small lateral dimension and small energy leakage into the hadronic calorimeter. These requirements were chosen so as to be 99% efficient for isolated electrons as measured in the test beam.

Two triggers were used to select $W^{\pm} \rightarrow e^{+}\nu(e^{-}\bar{\nu}\ )$ and $Z^{0} \rightarrow e^{+}e^{-}$. The *W trigger* requires an electromagnetic cluster with $E_t > 11.5$ GeV in the calorimeter while the *Z trigger* requires at least two electromagnetic clusters with $E_t > 5.0$ GeV and invariant mass above 10 GeV/c^2. In addition, a coincidence was required with the minimum bias trigger defined by the TOF hodoscopes.

The offline selection of *electron candidates* requires the following criteria to be satisfied :

1. A track must point to the electromagnetic cluster.
2. The lateral and longitudinal shower profiles must be compatible with those of an electron hitting the calorimeter in the position given by the track. The cut made is based on the ratio of the pulse heights on the two sides of the cell, energy sharing in the cells surrounding the hit cell, longitudinal shower profile and energy isolation.
3. There must be a preshower cluster associated to the track with $D^2 < 25$ (SFD) or $D^2 < 8$ (ECPT). Figure 4 shows the distribution in D^2 for SFD as obtained for central W candidates.
4. The preshower charge must exceed 2 MIP (minimum ionizing particle equivalents) in each projection in the SFD and 10 MIP in the ECPT. The preshower charge distributions for W candidates are shown in Fig. 5 a,b.

The efficiencies of the above cuts for electrons from W decays have been measured using a clean W sample, obtained by applying additional topological requirements, and releasing one cut at the time. The overall electron efficiency was estimated to be ~79% in the central region and ~73% in the end-cap region.

Figure 4. The distribution of D^2 (the normalised track-preshower distance squared) in the SFD for central W candidates. D^2 was required to be less than 25 for association.

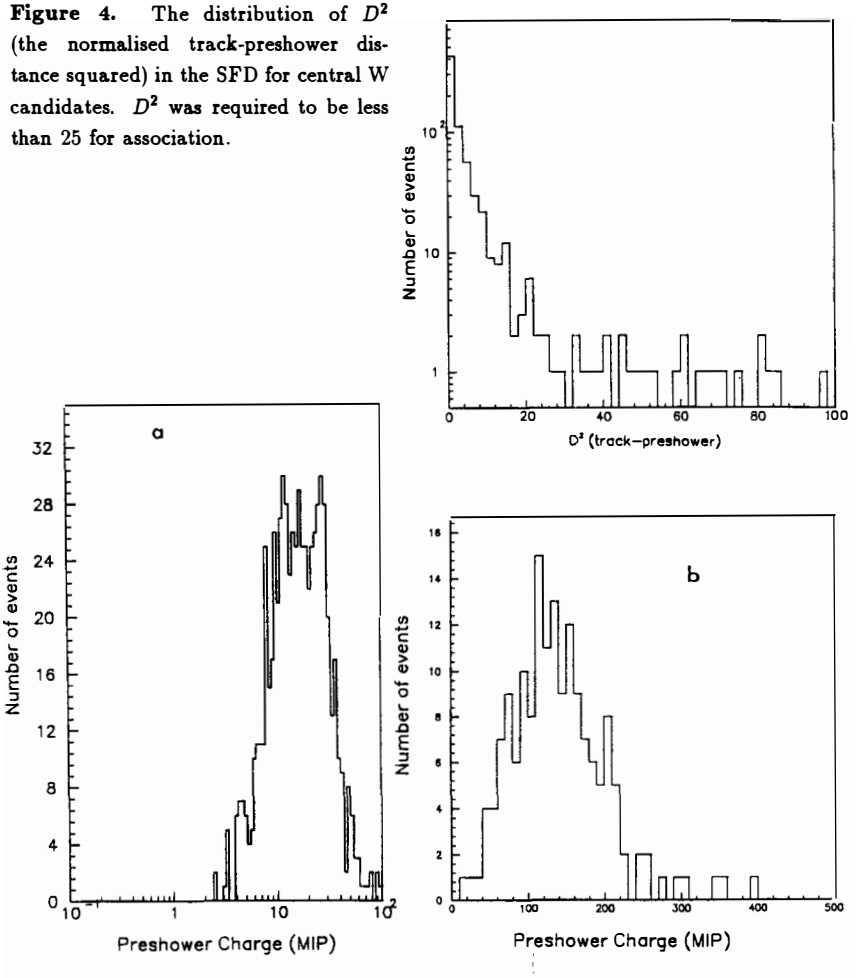

Figure 5. Preshower charge distribution for (a) central and (b) end-cap W candidates (figure 5a should be compared to figure 3).

4. The W sample

The $W \rightarrow e\nu$ event sample was selected as W triggers with the EM cluster satisfying the electron criteria discussed above and with $p_t^e, p_t^\nu > 20$ GeV/c (15 GeV/c in end-caps) The neutrino transverse momentum, p_t^ν, is defined as opposite to the vector sum of all transverse energy depositions in the calorimeter.[4] For events with the electron in the central calorimeter and $p_t^\nu > 20$ GeV/c the background of hadrons misidentified as electrons is estimated to be ~3%. Another background source, $W \rightarrow \tau\nu_\tau; \tau \rightarrow e\nu_\tau\nu_e$, contributes ~4%. The above estimates are preliminary. A more careful background evaluation, involving processing of large data samples, is required.

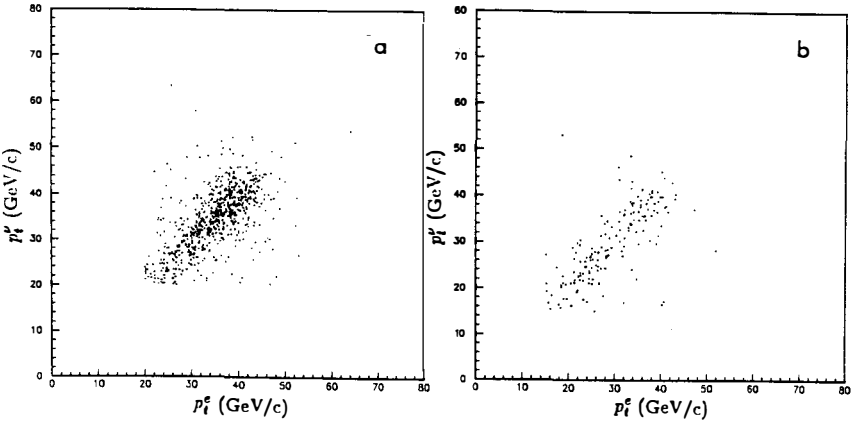

Figure 6. Transverse momentum (in GeV/c) of the neutrino versus that of the electron for (a) central and (b) end-cap W candidates.

Figures 6 a,b show scatter plots of p_t^ν vs p_t^e for events with the electron in the central and end-cap calorimeters (686 and 165 events), respectively. The distribution in transverse mass, $m_t(e,\nu) = \sqrt{2p_t^e p_t^\nu(1-\cos\phi_{e\nu})}$, of the central W candidates is shown in Fig. 7. From the previously published UA2 result[4]

$$\sigma(p\bar{p} \rightarrow W + X) \cdot \mathrm{Br}(W \rightarrow e\nu) = 570 \pm 40\ (\mathrm{stat}) \pm 70\ (\mathrm{syst})\ \mathrm{pb}$$

the expected number of central W events can be calculated. After correcting for the electron efficiency (Section 3), geometrical acceptance and integrated luminosity the expected numbers of events is 572 in good agreement with the 686 events observed (the sample of 686 events includes background as discussed above). The dominating systematic uncertainty in this calculation is a 10% error on the integrated luminosity. Systematic studies of efficiencies and background are in progress.

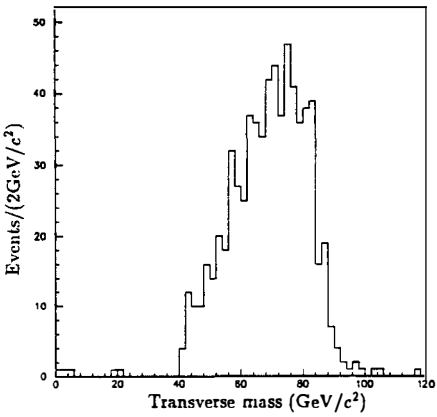

Figure 7. Transverse mass, $m_t(e,\nu)$, distribution for the central W candidates showing the characteristic jacobian peak.

5. The Z^0 sample

A fast filter selects events with two (or more) electromagnetic clusters with invariant mass above 40 GeV/c^2. These criteria are satisfied by 2737 events. The invariant mass distribution of these events (EM-EM sample) is shown in Fig. 8a. A fit of the form $m^{-\alpha}$ + *Gaussian* describes background and signal very well. The fitted number of events in the Z^0 peak is 112. The expected number of events in the peak, calculated from the previously published UA2 result[4]

$$\sigma(p\bar{p} \rightarrow Z^0 + X) \cdot Br(Z^0 \rightarrow e^-e^+) = 73 \pm 14 \text{ (stat)} \pm 7 \text{ (syst) pb}$$

correcting for the trigger efficiency, the geometrical acceptance and the integrated luminosity, is 95.

Requiring at least one identified electron (e-EM sample) or two identified electrons (e-e sample) results in the invariant mass distributions of Fig. 8b,c. The background under the signal in these plots can be estimated from the rejection measured in a background region (43 to 70 GeV/c^2) by rescaling the background under the signal in the EM-EM sample. The number of events at low masses (below 70 GeV/c^2) is compatible with the number expected from Drell-Yan e^-e^+ pairs.

An independent estimate of the efficiency of the electron cuts can be extracted from the ratio of the numbers of events in the signal region (above 73 GeV/c^2) in the e-e sample and the e-EM sample. The efficiencies measured by this method are 0.76 $\pm$ 0.05 in the central region and 0.85 $\pm$ 0.06 in the end-cap region (where the errors given are purely statistical). This is in reasonable agreement with the efficiencies measured for the W sample (Section 3). Using the efficiencies calculated from the Z^0 analysis the expected

number of events in the e-EM sample and e-e sample can be calculated as 90 and 57, respectively (to be compared with 91 and 62 observed above 73 GeV/c^2). These results show that the Z^0 cross-section is in good agreement with the previously published UA2 value. Further studies of efficiencies and background contributions are in progress.

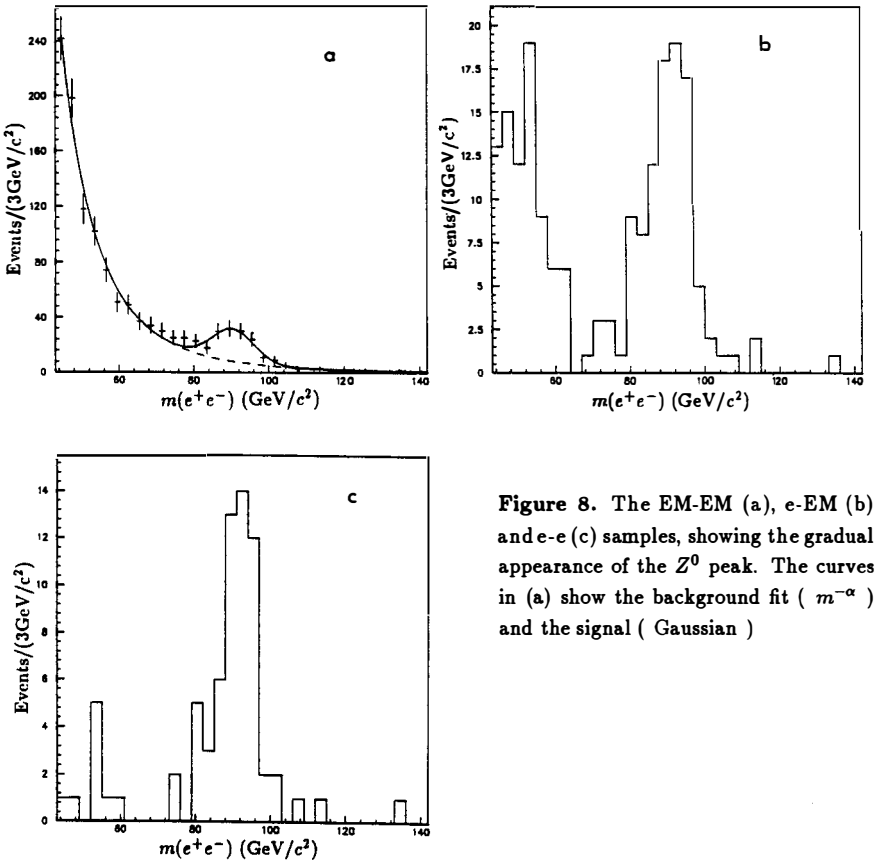

Figure 8. The EM-EM (a), e-EM (b) and e-e (c) samples, showing the gradual appearance of the Z^0 peak. The curves in (a) show the background fit ($m^{-\alpha}$) and the signal (Gaussian)

6. Mass and Width measurements

To determine the masses of the W and Z^0 a maximum likelihood fitting procedure has been developed. For suitable kinematical variables the expected spectra are determined using a fast Monte-Carlo program. By varying the boson mass and width in this simulation the likelihood for the observed data can be calculated as a function of the physical quantities and the values which maximise the likelihood can be found. This analysis is still too preliminary to quote mass values, since a large number of systematic effects need to be better understood.

In the case of $Z^0 \rightarrow e^+e^-$ the invariant mass of the electron pair can be used directly in the fit, while for the decay $W \rightarrow e\nu$ one has to rely on variables such as the transverse momentum of the electron or the transverse mass, $m_t(e,\nu)$. In the Z^0 case the systematic error on the mass is completely dominated by the error on the energy scale of the electromagnetic calorimeter for high energy electrons, while for the W there are additional systematic effects such as theoretical uncertainties in the p_t^W distribution and in the measurement of p_t^W as the negative vector sum of hadronic E_t. The latter measurement requires understanding the calorimeter response to low energy hadrons and E_t losses outside the calorimeter acceptance close to the beam axis. The width measurements suffer from a large uncertainty in the unfolding of the calorimeter resolution which is comparable to the widths themselves.

To reach the desired 1% accuracy the electromagnetic energy reconstruction must take into account the measured variation of the response across the cell surface as shown in Fig. 9.

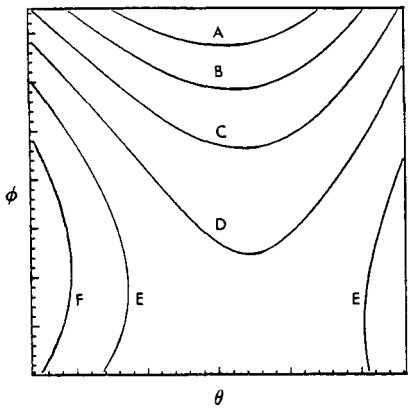

Figure 9. Contour plot showing the energy response for electrons as a function of ϕ and θ inside a half-cell in the central calorimeter. The lines (A,B,C,D,E,F) correspond to responses of 83, 89, 94, 99, 106, 114 %, respectively.

The measurement of hadronic p_t, necessary for fitting $m_t(e,\nu)$, is substantially improved in the upgraded UA2 with the addition of the end-caps. Figure 10a shows that the x-component of the measured p_t, in events selected by triggering on total transverse energy,

now has negligible non-gaussian tails. With p_x and p_y normally distributed, $p_t^2 = p_x^2 + p_y^2$ is distributed according to an exponential, i.e. $\propto e^{-p_t^2/\Delta^2}$ (Fig. 10b). Figure 10c shows how Δ grows with the total E_t in the event. The application of these results to the measurement of the (non-zero) p_t^W is non-trivial, and requires a careful analysis.

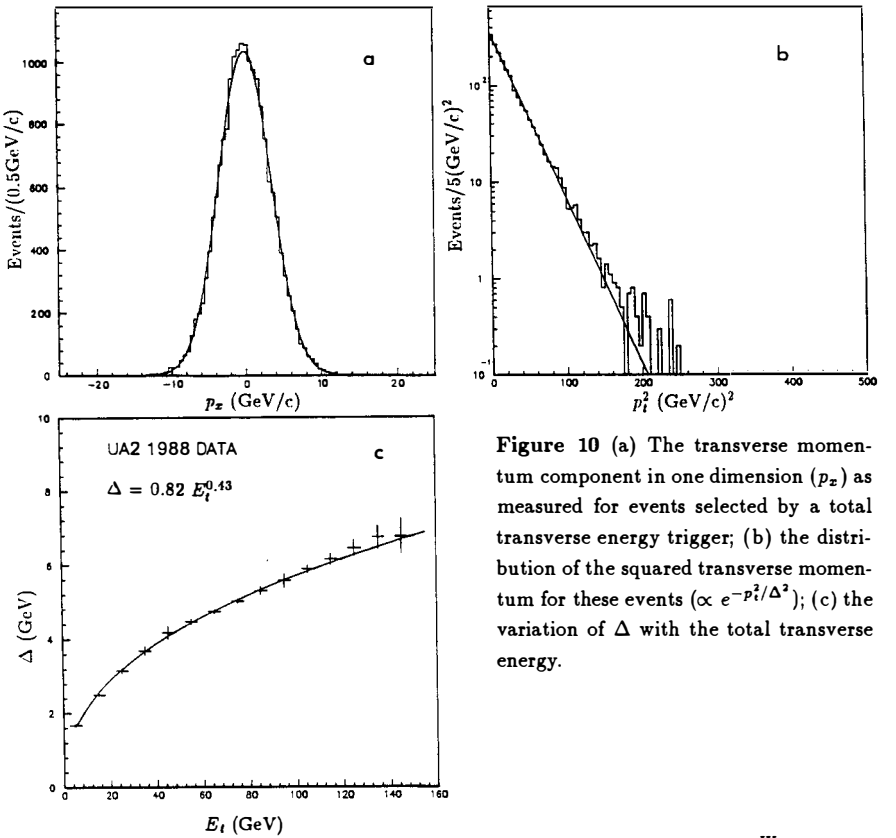

Figure 10 (a) The transverse momentum component in one dimension (p_x) as measured for events selected by a total transverse energy trigger; (b) the distribution of the squared transverse momentum for these events ($\propto e^{-p_t^2/\Delta^2}$); (c) the variation of Δ with the total transverse energy.

When fitting p_t^e rather than $m_t(e,\nu)$ one is insensitive to the measured p_t^W but relies instead on the theoretical prediction[5] for p_t^W used in the Monte-Carlo simulation. As can be seen from Fig. 11 this is in reasonable agreement with the data.

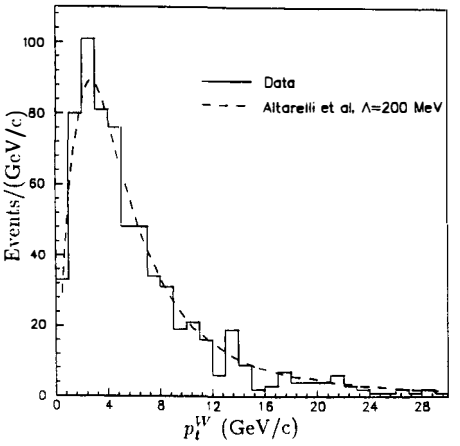

Figure 11. The measured p_t^W (solid line). The dashed line shows the distribution expected from theory, taking into account the detector resolution.

In addition to the studies mentioned above, consistency checks are being made using less optimal kinematical variables such as p_t^ν and varying the Monte-Carlo parameters (both theoretical input and detector model). The effects of the backgrounds mentioned in Section 4 on the observed spectra are also being investigated.

7. Conclusions

The preliminary results from the 1988 CERN $p\bar{p}$ collider run show that the UA2 detector behaves according to expectation. First estimates of W and Z^0 production rates are in good agreement with previously published UA2 results. Further systematic studies of efficiencies, background and calorimeter response are necessary before firm cross-sections and mass values can be derived.

REFERENCES

1. C.N.Booth, Proc. 6th Topical Workshop on Proton- Antiproton Collider Physics, Aachen, 1986 (World Scientific, Singapore, 1987) p. 381
2. E.Jones, Proc. 6th Topical Workshop on Proton- Antiproton Collider Physics, Aachen, 1986 (World Scientific, Singapore, 1987) p. 691
3. R.E.Ansorge et al., Nucl. Instr. and Meth. **A265** (1988) 33; R.E.Ansorge et al., Performance of the Scintillating Fibre Detector in the upgraded UA2 detector, to be published in Nucl. Instr. and Meth.
4. R.Ansari et al., Phys. Lett. **186B** (1987) 440
5. G.Altarelli, R.K.Ellis, M.Greco and G.Martinelli, Nucl. Phys. **B246** (1984) 12; G.Altarelli,R.K.Ellis and G.Martinelli, Z Phys. **C27** (1985) 617.